Origin and impact of initialisation shocks in coupled atmosphere-ocean forecasts

Article

Supplemental Material

Supplementary Information for

Origin and impact of initialisation shocks in coupled atmosphere-ocean forecasts

David P. Mulholland, Patrick Laloyaux, Keith Haines
and Magdalena Alonso Balmaseda

1 Confidence intervals for differences between experiments

In several of the figures shown in the main text and here in the Supplementary Information, confidence intervals for both RMSE and ACC are calculated for the differences between each uncoupled-initialised forecast type (i.e. U1, M1, M2 or M3) and C1, which is used as a baseline case, to estimate the uncertainty in these differences that arises due to sampling error with the 30-date ensemble. A non-parametric bootstrapping approach is used [following Goddard et al., 2013, Smith et al., 2013]. In this procedure, at each gridpoint, 100 synthetic 30-date forecast ensembles are created using random sampling with replacement, RMSE or ACC is calculated for the two experiments being compared, the differences between the two are sorted, and the 5^{th} and 95^{th} percentiles are located. A difference is taken as being significant if these upper and lower limits have the same sign. Where regional averages in RMSE or ACC are shown, upper and lower limits are calculated at each gridpoint and then spatially averaged. This method is likely to underestimate the uncertainty around each individual skill score, since the 30-date ensemble, although it does sample the seasonal cycle in three distinct periods, does not cover the full range of possible meteorological scenarios (e.g., interannual variability due to ENSO). Nonetheless, it should be a reliable estimate of uncertainties in the difference in skill scores between the various experiments, within the space spanned by this 30-date ensemble. Assessments of significant skill differences should not be over-interpreted, but are useful as an aid to understanding the comparisons between experiments.

2 Impact of initialisation shock on the seasonal timescale

The appearance of initialisation shocks in the ocean (Fig. 6) raises the possibility that the impact of these shocks could extend beyond the 10 days of the forecasts presented in the main text. Shock signals in the ocean subsurface have the potential to propagate on monthly timescales, potentially impacting near-surface forecasts at longer leads. The generation of spurious subsurface waves in the tropics could be especially problematic since it is such waves, when correctly initialised, that provide the means for skilful seasonal forecasts [Segschneider et al., 2001].

To investigate this possibility, three pairs of 7-month forecasts were also performed, beginning on 1 May 2008, 1 Jan 2009 and 1 Sep 2010, in accordance with the forecast periods used in the main text. Each hindcast was run as an ensemble of 5 members, with initial state perturbations applied in the atmosphere only. One hindcast in each pair was of type M1, and the other was of type M3; thus, the pair differed in the initial conditions used in the ocean, and in the consistency of ocean model versions between analysis and forecast.

Fig. S5 shows the difference in 20°C isotherm depth (M1 − M3) in the Pacific, averaged over the range 2–8°N, which is where equatorial Rossby waves are most prominent [Chelton et al., 2003], in each of the three seasonal forecasts. In the 1 January 2009 forecasts, westward-propagating signals, with phase speeds consistent with those of Rossby waves ($\sim 10^\circ$ month^{-1}), are evident, and differences remain significant at the 90% level out to a lead time of 4–5 months. Forecasts initialised in January 2009 all showed large SST shocks in the eastern Pacific in M1 (Fig. 6), and the negative isotherm depth anomaly seen here in M1 (relative to M3), which is larger than differences present in the initial

conditions, is consistent with the initial surface cooling. While similar, albeit weaker, wave signals are evident in the 1 September 2010 forecast difference, the 1 May 2008 shows no such signals emanating from the eastern Pacific, which is consistent with the smaller Niño3 SST shock seen in the first few days in the Apr–May 2008 short-range forecasts (Fig. S2(a)).

Rossby wave signals, propagating westward, are prominent in these forecasts due to the occurrence of the largest initialisation in the eastern parts of the Pacific and Atlantic basins, but there is also some evidence of Kelvin waves propagating along the equator (not shown) over 2–3 months, at least in the 1 January 2009 forecast. Both of these wave modes have the potential to retain memory of an initialisation shock following a change in ocean model, over a period of several months.

SST differences, averaged on the equator, are shown in Fig. S6. Again it is seen that differences at month 1 are much larger than the differences in the initial conditions (month 0); that these differences are less substantial in the 1 May 2008 forecasts, which show a smaller initialisation shock; and that the differences can propagate westward, at phase speeds consistent with the Rossby waves identified above. There are signs of links with the signals in thermocline depth difference, though these do not explain the SST differences entirely. The existence of significant differences in SST after several months suggests that initialisation shock can affect both the atmosphere and the ocean on the seasonal timecale.

Long-lived signals resulting from initialisation shock could, on the seasonal timescale, either enhance or reduce systematic model biases, depending on the signs of the two components. However, their presence can at least be expected to complicate the calculation of lead-time-dependent bias correction terms, and therefore it seems plausible that the occurrence of initialisation shocks in the

ocean, particularly in tropical regions, may degrade the skill of seasonal forecasts of SST and related variables; though with only three forecast start dates, we cannot evaluate this here.

References

D. B. Chelton, M. G. Schlax, J. M. Lyman, and G. C. Johnson. Equatorially trapped Rossby waves in the presence of meridionally sheared baroclinic flow in the Pacific Ocean. *Prog. Oceanogr.*, 56(2):323–380, 2003.

L. Goddard, A. Kumar, A. Solomon, D. Smith, G. Boer, P. Gonzalez, V. Kharin, W. Merryfield, C. Deser, S. J. Mason, et al. A verification framework for interannual-to-decadal predictions experiments. *Clim. Dyn.*, 40(1-2):245–272, 2013.

J. Segschneider, D. L. T. Anderson, J. Vialard, M. Balmaseda, T. N. Stockdale, A. Troccoli, and K. Haines. Initialization of seasonal forecasts assimilating sea level and temperature observations. *J. Climate*, 14(22):4292–4307, 2001.

D. M. Smith, R. Eade, and H. Pohlmann. A comparison of full-field and anomaly initialization for seasonal to decadal climate prediction. *Clim. Dyn.*, 41(11-12):3325–3338, 2013.

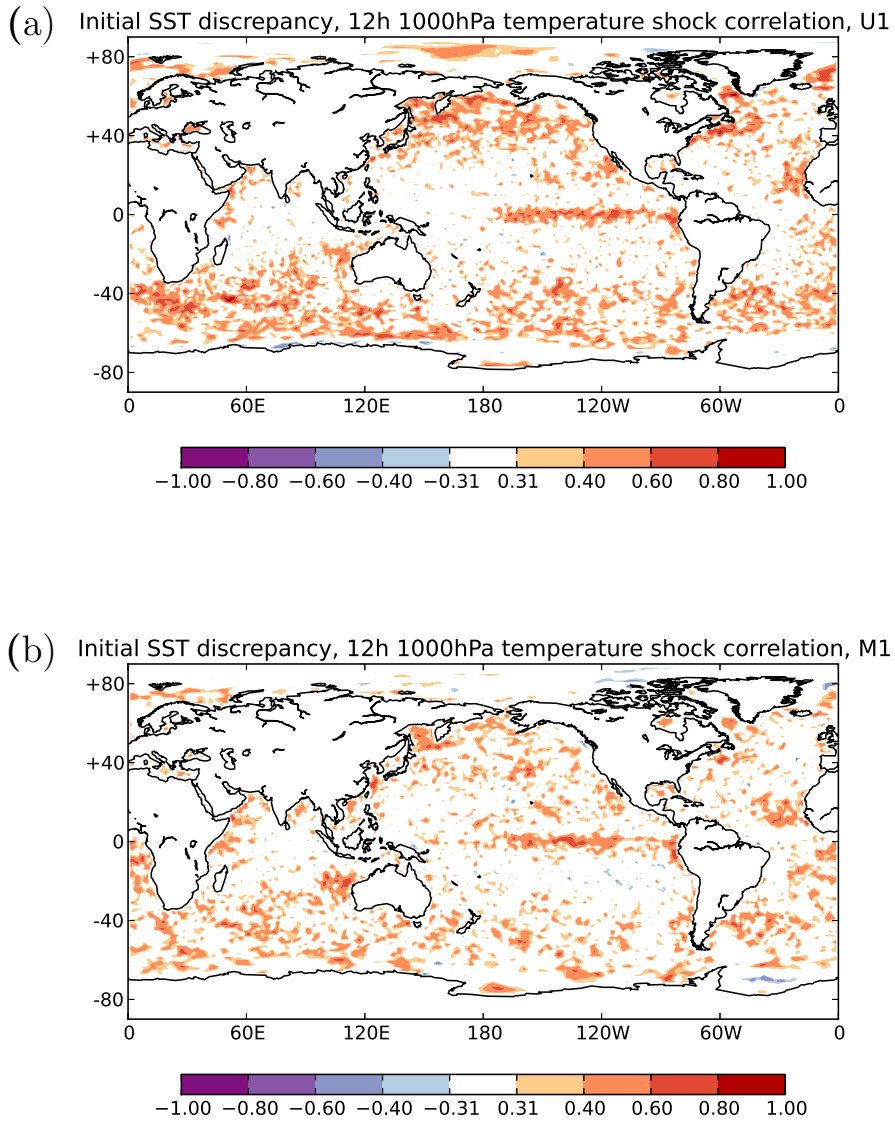

FIG. S1: Correlation between the difference in SST in the atmospheric and ocean analyses at 0 h forecast lead time, and the 'shock' component of the forecast 1000 hPa temperature error (the raw error, rather than the RMSE) at 12 h lead time, for forecasts U1 (a) and M1 (b). A correlation of ±0.31 is significant at the 90% level. Positive correlations indicate that the atmospheric temperature error after 12 h was of the same sign as the change in SST forcing experienced from analysis to forecast (i.e. from gridded observed SST to U_ocean/ORAS4).

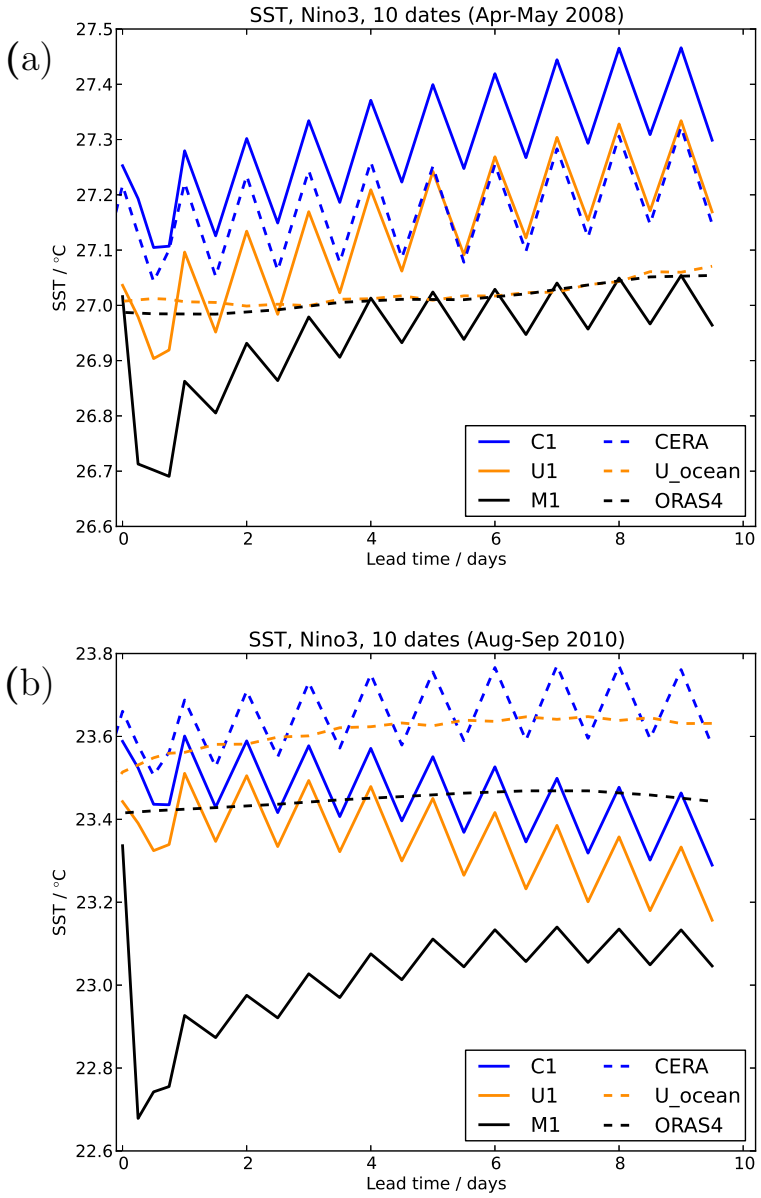

FIG. S2: Niño3 (150–90°W, 5°N–5°S) SST forecast and analysis time series for the average of the 10 start dates in Apr–May 2008 (a) and Aug–Sep 2010 (b). Forecast series are plotted at (0, 6, 12, 18, 24) hours, and every 12 hours thereafter; analysis series for CERA and U_ocean are plotted at the same frequency, but only daily means are plotted for ORAS4.

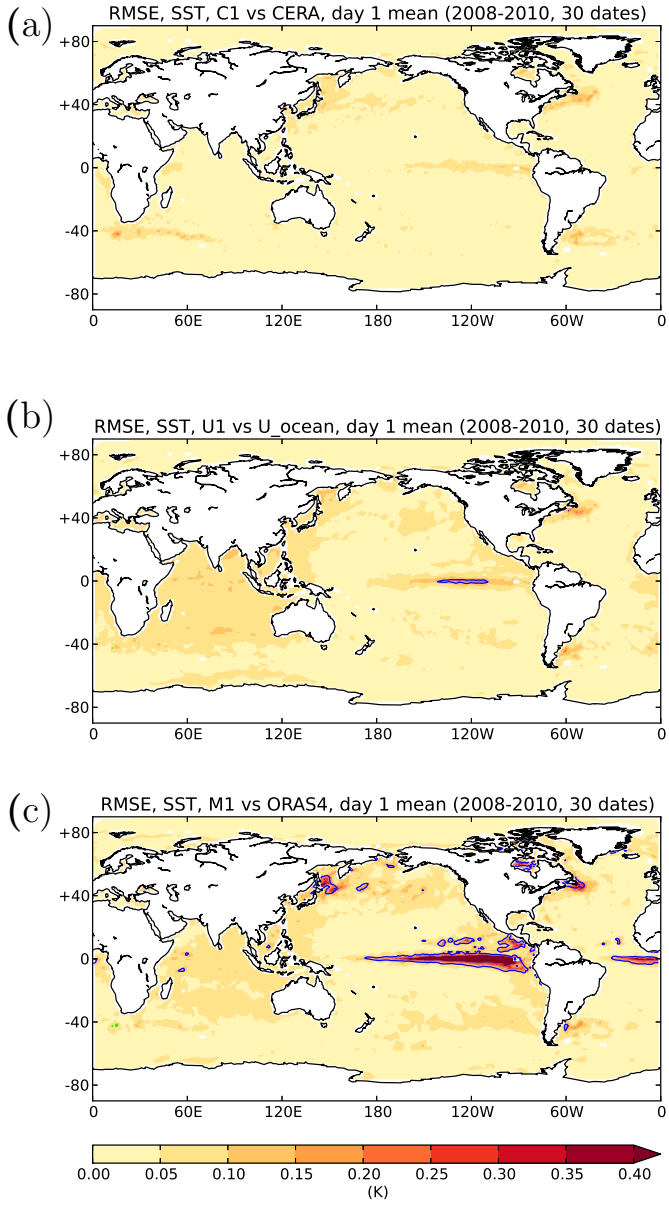

FIG. S3: SST forecast RMSE, relative to the analysis used as the initial conditions, for C1 (a), U1 (b) and M1 (c), for daily mean forecast values from the first day. Contours in (b) and (c) show differences in RMSE relative to C1, with blue (green) contours marking increased (decreased) RMSE in U1 and M1. Contours are drawn at a difference of 0.1°C. Only differences that are significant at the 90% level, estimated using the bootstrapping method, are contoured.

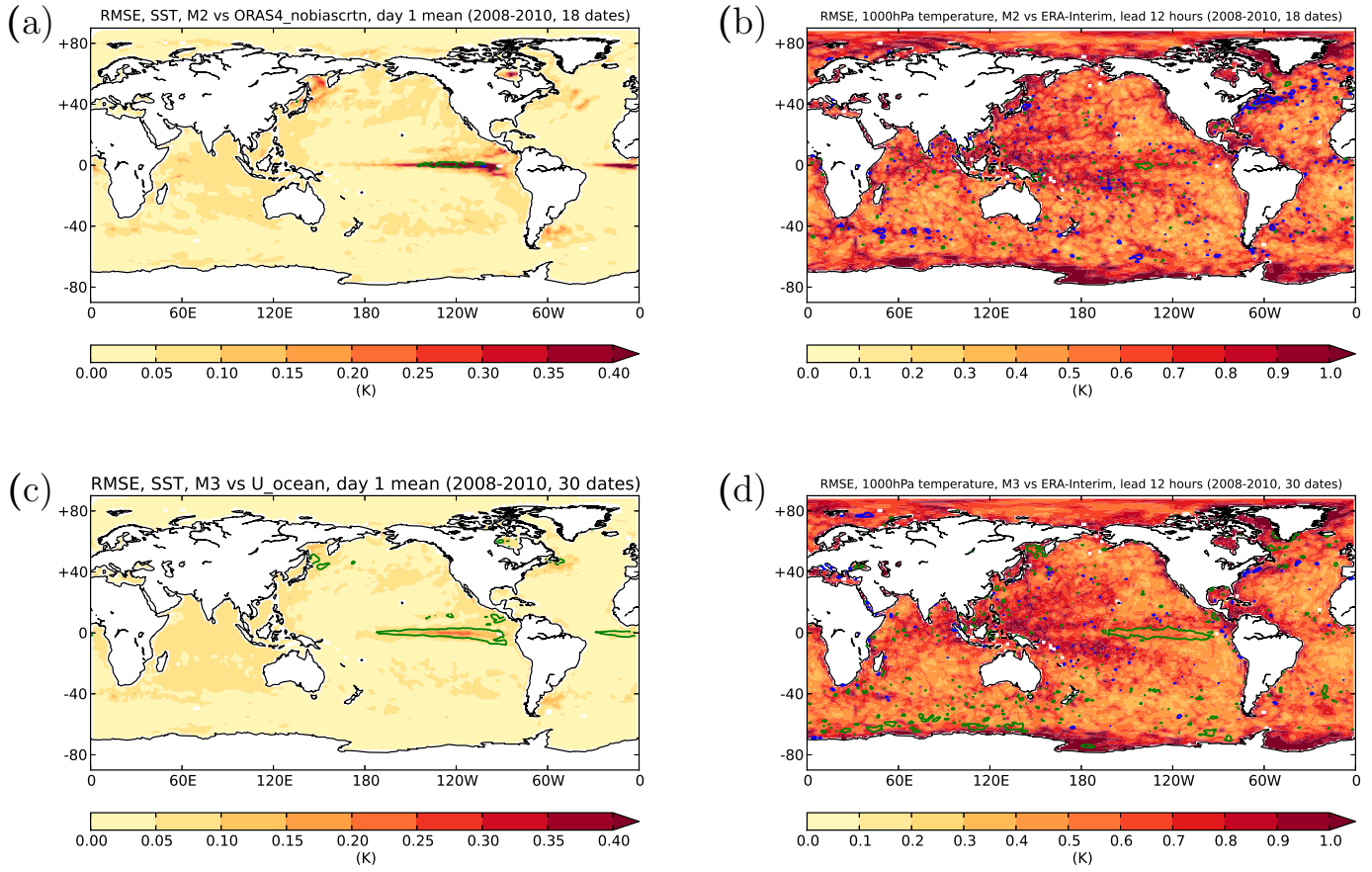

FIG. S4: SST and 1000 hPa air temperature RMSE for M2 (a,b) and M3 (c,d), as in Figs. S3 and 3, except that contours now show differences in RMSE relative to M1, with blue (green) contours marking larger (smaller) RMSE in M2 or M3. Contours are drawn at differences, significant at the 90% level, of 0.15°C in (a,c) and 0.1°C in (b,d).

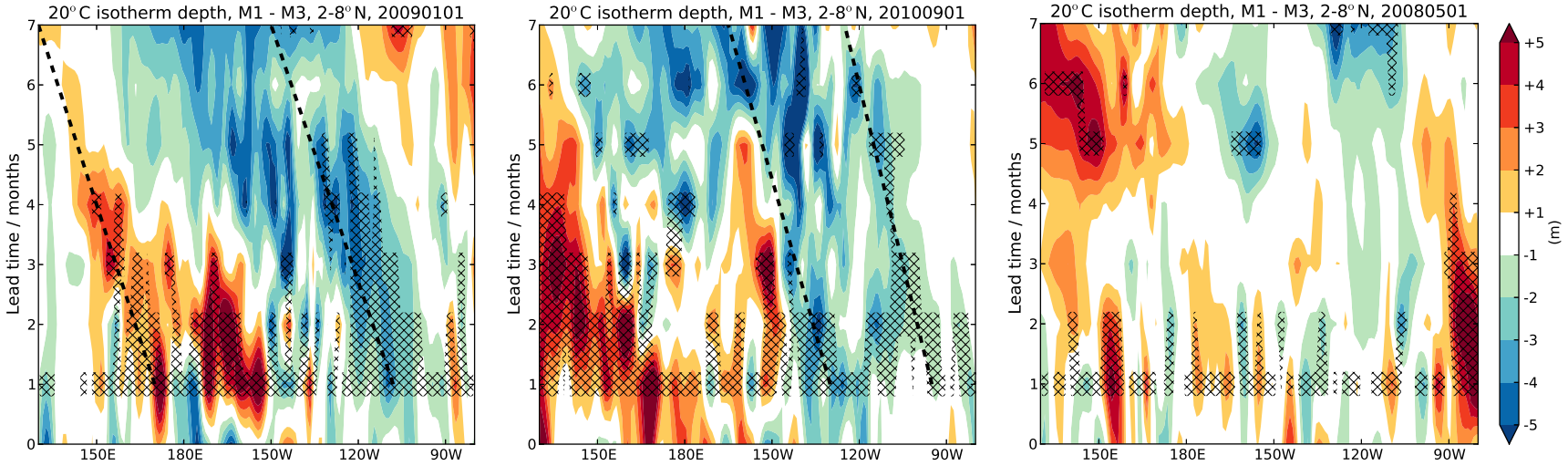

(a) (b) (c)

FIG. S5: Difference in the depth of the 20°C isotherm (in metres) between M1 and M3, averaged between 2°N and 8°N, for the seasonal 1 January 2009 (a), 1 Sep 2010 (b) and 1 May 2008 (c) forecasts. Forecast data are plotted as monthly means, starting at lead time 1 month; the difference between the initialising analyses (ORAS4 − U_ocean) for December 2008 is plotted at lead time 0, to show that difference in the forecasts' initial conditions are non-zero, but smaller than differences by the first forecast month. Hatching (beginning at month 1) marks ensemble-mean differences that are significant at the 90% level, using a t-test. Dashed lines highlight the propagation of possible Rossby wave signals, generated by initialisation shock, at phase speeds of $\sim 10^\circ$ month^{-1}.

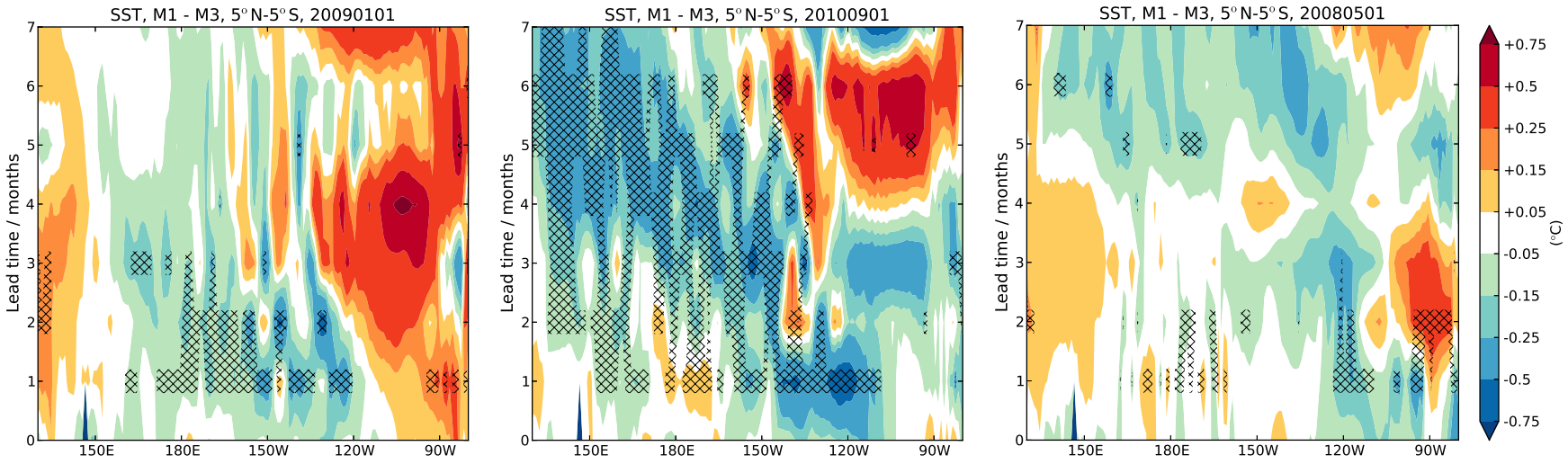

(a) (b) (c)

FIG. S6: As in Fig. S5, but for SST averaged over 5°N–5°S. As in the previous plot, it can be seen that larger differences (not present at month 0) form in the first month in the cases in which the initialisation shock is larger (20090101 and 20100901), and these differences can be maintained over seasonal timescales (20100901).